machines

MDPI

Article

CNN-KAN Hybrid Driven Intelligent Vibration Machinery and Vibration State Recognition Method of Edge Deployment

Tianlong Wang [1], Xinwei Wang [2,*], Shihao Hu [2], Shixuan Yang [3,*], Zhaohui Cai [1], Buqiao Fan [2], Tong Xiang [2] and Muhammad Moman Shahzad [4]

[1] CSCEC City Construction Development Co., Ltd., Beijing 100037, China; wtlong@mail.nwpu.edu.cn (T.W.); czhcscec@163.com (Z.C.)
[2] School of Civil Engineering and Communication, North China University of Water Resources and Electric Power, Zhengzhou 450045, China; 202408424@stu.ncwu.edu.cn (S.H.); buqiao@mail.nwpu.edu.cn (B.F.); 202508005@stu.ncwu.edu.cn (T.X.)
[3] Kang-Ju Construction Parts Certification Center, Centre of Science and Technology Industrial Development, Ministry of Housing and Urban-Rural Development of the People's Republic of China, Beijing 100835, China
[4] Department of Civil Engineering, National University of Sciences and Technology, Balochistan Campus, Quetta 86000, Pakistan; m.momin@nbc.nust.edu.pk
* Correspondence: wangxinwei@ncwu.edu.cn (X.W.); yangsxuan@stu.hqu.edu.cn (S.Y.)

Abstract

Concrete vibration quality has an outsized effect on structural durability, but construction sites have no reliable way to monitor it in real time. Compounding this, vibration machinery has no self-awareness of its own operating state, so failures and degradation tend to go unnoticed until something goes wrong. The proposed system integrates a Raspberry Pi controller and a hybrid neural network model within the vibrator apparatus itself. The model pairs a 1D CNN with a Kolmogorov–Arnold Network (KAN). The CNN initially conducts the majority of the computational workload: it systematically reduces dimensionality and extracts salient features from extensive time-series data, thereby circumventing the convergence challenges that a KAN encounters when processing unrefined high-dimensional sequences independently. Subsequently, a B-spline-based classification module supersedes the conventional fully connected layer. This innovation is noteworthy; the module is capable of identifying minute damping variations and frequency alterations during the process of concrete liquefaction, accurately distinguishing between states such as "adequate compaction" and "over-vibration," which may appear nearly indistinguishable in their dynamic responses. The achieved accuracy in vibration state classification was 97.55%, while recognition of no-load conditions reached 98.17%. The system provides millisecond-level active protection against hazardous impacts, effectively reducing equipment wear. With a low implementation cost of approximately 800 RMB and a projected 20% improvement in construction compliance, this work provides reliable technical support for ensuring controllable construction quality and extending equipment service life, offering an efficient solution for the intelligent upgrade of building equipment.

Keywords: vibration machinery; real-time vibration monitoring; vibration state classification; hybrid neural network; Kolmogorov–Arnold network

Check for updates

Academic Editor: Tamara Nestorović

Received: 13 April 2026
Revised: 2 May 2026
Accepted: 4 May 2026
Published: 7 May 2026

Copyright: © 2026 by the authors. Licensee MDPI, Basel, Switzerland. This article is an open access article distributed under the terms and conditions of the Creative Commons Attribution (CC BY) license.

1. Introduction

In modern concrete engineering, the accurate identification of the vibration state is critical for ensuring structural safety and durability, directly dictating the density and

homogeneity of the material [1]. Traditional construction predominantly relies on manual experience, which often leads to internal porosity defects like honeycombs due to "under-vibration" or aggregate segregation caused by "over-vibration" [2]. In tunnel engineering, vault cavities are common defects closely related to insufficient pouring compactness [3]. Consequently, substantial research has been conducted: Yang et al. identified a linear relationship between vibration acceleration and porosity [4]; Zheng et al. proposed biaxial vibration mixing to improve overall concrete quality [5]. However, the intrinsic lack of self-perception in standard equipment often causes diagnostic accuracy to plummet under variable speeds [6]. More critically, the harsh construction environment and high-speed operation make vibrating rods prone to mechanical fatigue during frequent idling or collisions with rigid molds, resulting in uncontrollable quality and high equipment depreciation.

The convergence of machine learning and civil engineering has shifted monitoring from "post-sampling inspection" to "real-time early warning." Within damage detection and state assessment, techniques such as YOLOv7-based crack identification [7], precision localization algorithms [8], deep learning-driven mechanical damage assessment [9], and genetic algorithm-based state forecasting [10] have demonstrated significant potential. To sharpen feature extraction, the integration of STFT with SVM has enabled damage detection [11], and multi-task fusion networks have been developed for complex scenes [12]. Furthermore, real-time monitoring coupled with finite element modeling [13,14] and nonlinear dynamics modeling [15] has established a foundation for addressing complex systems. For small-sample scenarios, lightweight diagnosis frameworks have exhibited high fidelity [16,17], while navigation algorithms for dynamic environments offer insights into sensor motion compensation [18]. Nevertheless, the computational intensity of these models often precludes their millisecond-level execution on micro-nodes embedded within vibrating rods, and research regarding active protection mechanisms for equipment safety remains remarkably scarce.

The emergence of convolutional neural networks (CNN) and Kolmogorov–Arnold Networks (KAN) offers a promising trajectory for real-time identification in embedded environments. CNNs, characterized by weight-sharing mechanisms, have excelled in tool wear identification [19] and power supply risk assessment [20]. To further enhance the recognition precision for internal impact damage [21] and vibration response parameters [22] in concrete, KAN algorithms utilize learnable nonlinear activation functions to achieve superior fitting precision. In practical engineering, both follow standardized workflows to adapt to construction needs [23]. CNNs capture local features and filter noise efficiently [24,25], achieving recognition accuracies of up to 99.43% under complex benchmarks [26]. While stacking technologies [27], hybrid predictions [28], and kernel-method-optimized classifiers [29,30] further bolster performance, identifying transitional states with blurred physical boundaries—such as "compacted" versus "over-vibrated"—remains a formidable challenge for lightweight models attempting to capture subtle damping shifts caused by liquefaction.

In summary, to bridge the gap in intelligent equipment for "real-time quality monitoring" and "active asset protection," this study, inspired by robust identification strategies for complex environments [31], presents the development of an integrated intelligent vibration equipment featuring an onboard edge computing unit. This work achieves equipment "self-perception" through embedded sensing arrays and control modules; proposes a CNN-KAN hybrid architecture designed to enhance nonlinear mapping precision under constrained computational budgets; and establishes a millisecond-level active protection mechanism. By identifying hazardous conditions in real-time, the system effectively mitigates operational wear and extends the service life of the equipment, providing a robust technical foundation for the intelligent upgrading of construction machinery.

2. Intelligent Vibration Rod Equipment and Concrete Vibration State Test

2.1. System Architecture of the Intelligent Vibration Equipment

An intelligent concrete vibration monitoring system featuring embedded edge intelligence was developed, with its functional architecture illustrated in Figure 1. The system is synergistically driven by three core modules comprising the data acquisition terminal, the main control processing hub, and the multi-dimensional feedback unit. To withstand extreme mechanical vibrations and electromagnetic interference (EMI) typical of construction environments, the hardware employs an industrial-grade reinforcement scheme where a high-precision IM600 triaxial accelerometer (Ouhuayuan, Shenzhen, China) is hermetically encapsulated within a specialized damping chamber at the vibrator's head. This ensures the lossless transmission of 200 Hz raw signals to a Raspberry Pi 5 edge computing node via a 3 m RVVP 6 × 0.3 national standard shielded cable. The control hub utilizes this miniaturized node to employ a built-in CNN-KAN hybrid algorithm for instantaneous waveform interpretation. The feedback unit, integrated via a control bus to an industrial buzzer, provides millisecond-level acoustic alerts based on algorithmic decisions, establishing an edge-based closed-loop from raw data acquisition to intelligent response.

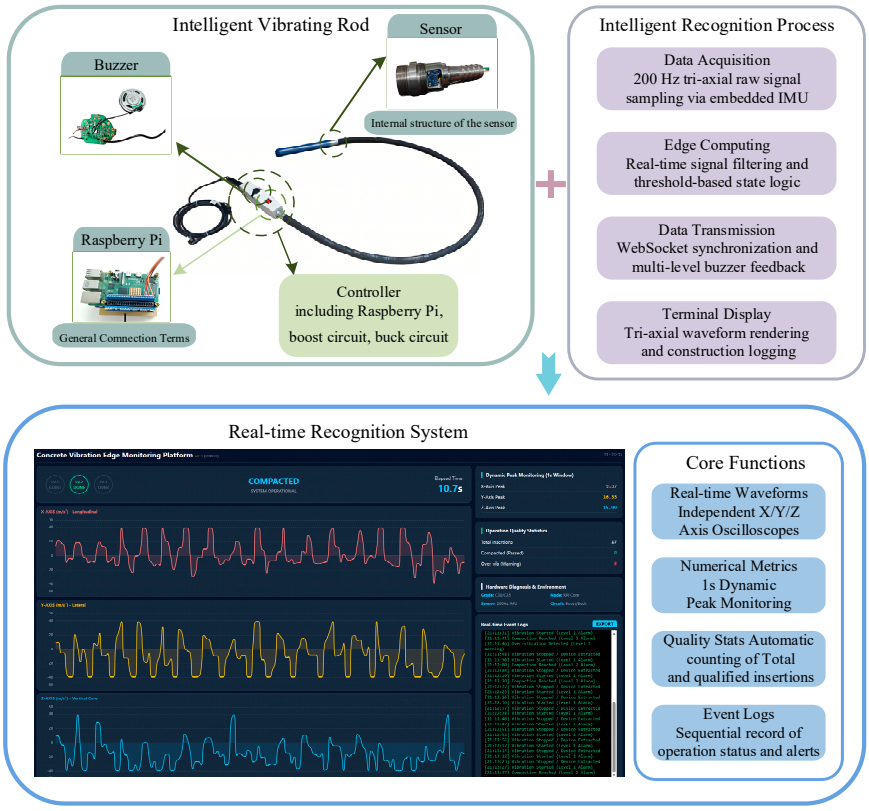


Figure 1. Schematic diagram of the intelligent concrete vibration monitoring system structure.

2.2. Concrete Vibration Performance Test and Equipment Protection Validation

To evaluate the synergistic performance of the equipment in both construction quality control and active asset protection, a comprehensive experimental workflow was designed, with the specific test phases depicted in Figure 2a–f. The procedure follows strict engineering standards, commencing with material preparation (Figure 2a) and standardized mixing (Figure 2b), followed by slump testing (Figure 2c) to verify that the concrete's workability aligns with experimental criteria.

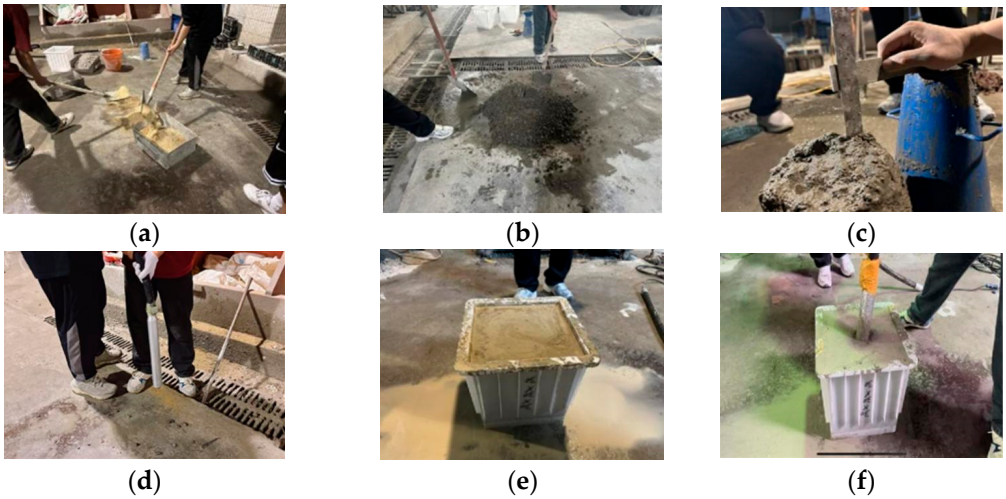


Figure 2. Schematic diagram of concrete vibration state test conditions. (**a**) Prepare experimental raw materials; (**b**) mix according to the steps; (**c**) measure slump; (**d**) collect air-vibration data; (**e**) load the mold; (**f**) vibrate and collect data.

The defining feature of the intelligent upgrade is the integrated active protection mechanism. Validation of this mechanism specifically focuses on the air-vibration data collection phase shown in Figure 2d. In this step, the system simulates idle vibration conditions representing high-wear scenarios. By identifying the energy distribution signatures of idle waveforms, the control unit triggers a millisecond-level acoustic alarm to alert operators, effectively preventing mechanical structure damage and thermal accumulation caused by prolonged idling.

Subsequently, the experiment proceeded to the mold loading (Figure 2e) and actual vibration (Figure 2f) phases. During this process, the system not only monitors quality-related states—"under-vibration," "compaction," and "over-vibration"—but also simulates Ground Impact scenarios involving instantaneous high-energy overloads when the vibrator head accidentally strikes rigid foundations or reinforcement meshes. All sensor signals, warning thresholds, and operational status labels were logged in real-time within a PostgreSQL database. This experimental sequence, spanning from idle protection to operational monitoring, provides a robust data foundation for evaluating the algorithm's robustness and the equipment's overall intelligent performance.

3. Concrete Vibration State Recognition Algorithm

3.1. Basic Principles of KAN

The Kolmogorov–Arnold Network (KAN) is a neural network model constructed based on the Kolmogorov–Arnold representation theorem. This theorem mathematically proves that any multivariable function can be represented as a combination of a finite number of single-variable functions. Its general mathematical expression is defined as:

$$f(x) = f(x_1, x_2, \cdots, x_n) = \sum_{q=1}^{2n+1} \Phi_q \left(\sum_{p=1}^{n} \phi_{q,p}(x_p) \right) \quad (1)$$

Among them $\phi_{q,p}$ is a one-dimensional function, and Φ_q is a composite function.

Unlike traditional multilayer perceptrons, which place weight parameters on the network 'nodes,' the core innovation of KAN is moving the learnable nonlinear activation functions to the network 'edges'.

Its typical network structure is shown in Figure 3. The network removes the originally fixed activation functions at the nodes and instead allows each edge to carry a learnable

univariate function $\phi_{q,p}$ (usually parameterized using B-spline curves). In traditional neurons, inputs are weighted by w and summed before passing through a fixed activation function σ; in KAN units, the input signal undergoes a functional transformation directly on the edge, and nodes only perform simple summation operations. This theoretically provides a more efficient, parameter-reduced method for function approximation. This high parameter efficiency significantly alleviates the reliance on large-scale memory, making KAN particularly suitable for deployment on resource-constrained edge computing platforms (such as the Raspberry Pi) embedded within the vibration equipment.

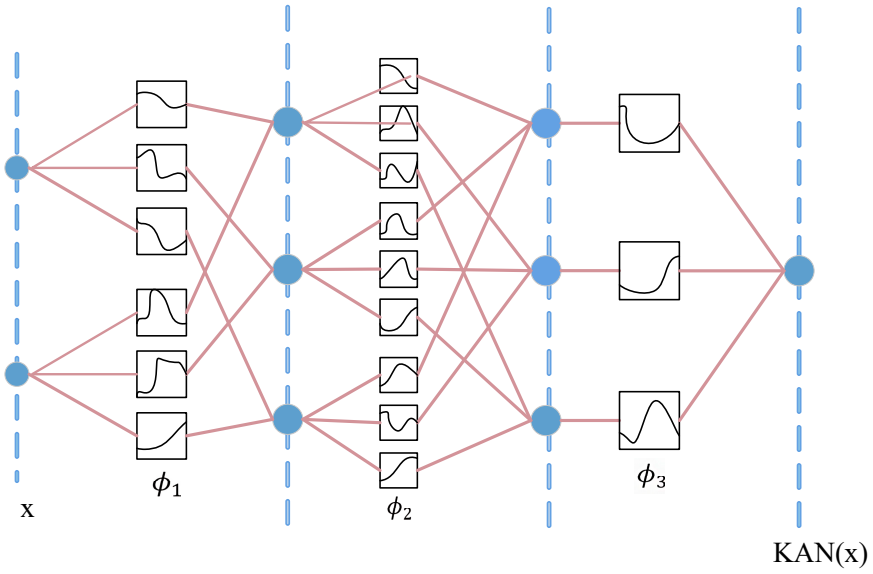


Figure 3. The network structure of KAN.

Univariate functions in KAN are usually parameterized using B-spline curves, which are easy to optimize. The mathematical definition of a B-spline is:

$$\text{spline}(x) = \sum_i c_i B_i(x) \tag{2}$$

In the formula, c_i is the trainable control vertex, and $B_i(x)$ is the corresponding B-spline basis function.

The computation at each layer in the network can be represented as:

$$x_{l+1} = \Phi_l x_l = \begin{pmatrix} \phi_{l,1,1}(\cdot) & \cdots & \phi_{l,1,n_l}(\cdot) \\ \vdots & \ddots & \vdots \\ \phi_{l,n_{l+1},1}(\cdot) & \cdots & \phi_{l,n_{l+1},n_l}(\cdot) \end{pmatrix} x_l \tag{3}$$

Among them ϕ_l is a matrix composed of all the activation functions in that layer. Consequently, the end-to-end output of the entire network is reflected as the composite operation of multiple layers of functions:

$$f(x) = (\Phi_{L-1} \circ \Phi_{L-2} \circ \cdots \circ \Phi_0)(x) \tag{4}$$

By introducing learnable functions on the connections, combined with regularization and structural optimization, KAN can accurately depict highly complex nonlinear mapping relationships with an extremely small number of parameters, enabling it to handle complex modeling scenarios with multi-feature input very well.

3.2. Basic Principles of CNN

Convolutional neural networks (CNNs) possess significant advantages in processing temporally correlated vibration signals due to their unique local perception and weight-sharing mechanisms. The CNN module constructed in this paper is mainly responsible for extracting deep features from the raw waveform, and its network structure is shown in Figure 4.

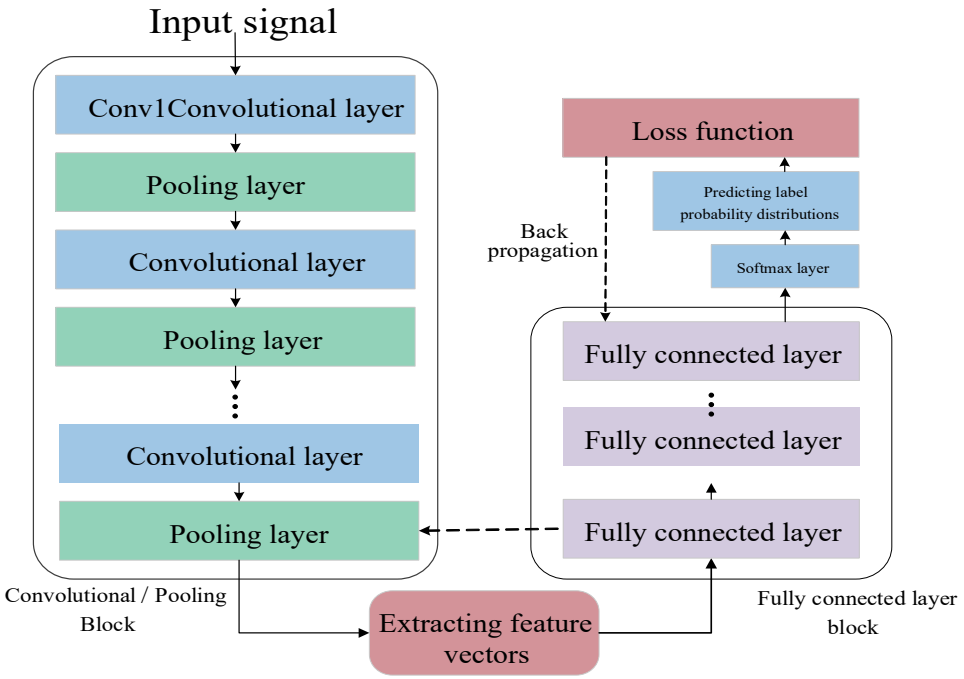


Figure 4. The network structure of CNN.

In the feature extraction stage, the convolution kernel captures the local temporal evolution characteristics of the signal by performing cross-correlation operations with the input signal. For the *j*-th feature map of the l-th layer, the mathematical calculation process of its output y_j^l is as follows:

$$y_j^l = \sigma\left(\sum_{i \in M_j} x_i^{l-1} \times w_{ij}^l + b_j^l\right) \tag{5}$$

Among them x_i^{l-1} is the feature map input from the previous layer, w_{ij}^l is the learnable convolution kernel weight, b_j^l is the bias term, and the symbol $\times$ denotes the one-dimensional convolution operation.

In order to adapt to the inherently non-stationary characteristics of concrete vibration signals, this paper provides targeted approaches in the convolutional layer parameters. The first convolutional layer uses 13 convolution kernels of size three, aiming to first capture the basic shape characteristics in the original waveform; the second convolutional layer uses 23 convolution kernels of size two, to extract the detailed features of high-frequency fluctuations in the signal with the help of a more refined receptive field.

In order to ensure the stability of model training and accelerate convergence efficiency, a Batch Normalization (BN) layer is introduced after the convolution operation. By centering and scaling each batch of data, the computational logic of the BN layer is:

$$\hat{x} = \frac{x - \mathbb{E}[x]}{\sqrt{\mathrm{Var}[x] + \epsilon}} \tag{6}$$

$$y_{\mathrm{BN}} = \gamma \hat{x} + \beta \tag{7}$$

Here, $E[x]$ and $Var[x]$ are the mean and variance, respectively. The normalized signal is then mapped through the ReLU activation function $f(x) = \max(0, x)$. This design not only enhances the nonlinear expressive capability of the network but also, by utilizing its sparse activation characteristics, alleviates the problem of gradient vanishing in deep networks to some extent.

The pooling layer reduces the spatial dimensions through a down-sampling operation, thereby decreasing the number of model parameters and improving its robustness to signal shifts. This architecture adopts a max-pooling strategy to extract the maximum activation within a specific sliding window Ω:

$$p_j^l = \max_{k \in \Omega} \left(a_{jk}^l \right) \tag{8}$$

Among them a_{jk}^l is the activation value of the neuron within the pooling window. After multiple layers of convolution and pooling iterations, the original vibration signal is transformed into a highly condensed feature vector, which is finally connected to the classification module through a global average pooling layer.

3.3. Data Preprocessing

3.3.1. Data Augmentation

The original vibration waveforms measured on construction sites often have long time-series characteristics. Directly inputting them all into the model for processing can result in significant overhead. To address this situation, this study uses the sliding window method to segment the original signals. This technique uses a fixed-length window and step size to set the segmentation, ensuring that the continuity of the physical characteristics of the signal is not interrupted, transforming the long time series into multiple short samples of equal length. The specific segmentation process is shown in Figure 5.

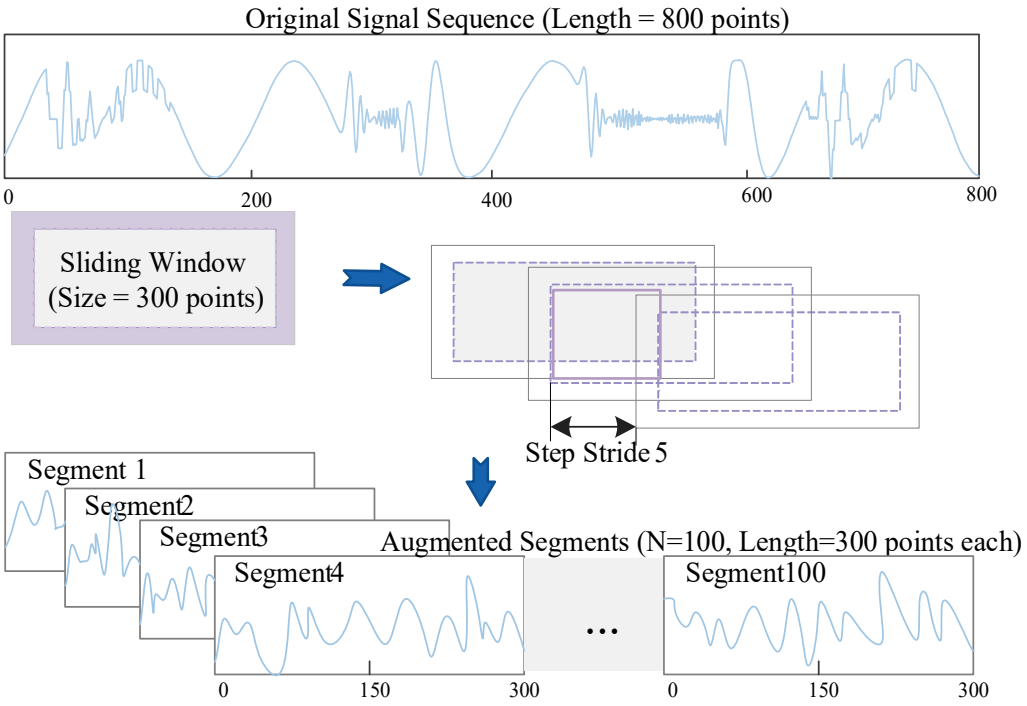


Figure 5. Schematic diagram of sliding window data augmentation.

Sliding window augmentation not only significantly expands the sample size, effectively mitigating the risk of overfitting that may arise from data scarcity, but also enhances the model's robustness to signal time-shift characteristics, laying a data foundation for the stable training of subsequent deep neural networks.

The signal segments after sliding window augmentation are the only data source for all subsequent algorithms. CNN-KAN and CNN directly extract the original temporal features within the segments, while KAN further needs to transform these segments into statistical feature vectors.

3.3.2. Feature Extraction and Selection Strategy

To verify the classification performance of different algorithm architectures, this study designed a dedicated feature extraction process for the pure KAN model. Since the original vibration signals have high dimensionality and strong non-stationarity, directly inputting them into the KAN model would create tremendous computational pressure. Therefore, this study first converts the complex waveform signals into representative low-dimensional numerical indicators through feature extraction methods.

This study processes the original signals from both time and frequency domains, initially extracting 20 initial features, including variance, root mean square value, peak factor, and energy distribution in specific frequency bands. For specific feature names and calculation formulas, see Table 1.

Table 1. Definitions and formulas of time and frequency domain features.

Time Domain		Time Domain		Freq Domain		Freq Domain	
Name	**Formula**	**Name**	**Formula**	**Name**	**Formula**	**Name**	**Formula**
Mean	$\mu = \frac{1}{N}\sum_{t=1}^{N} x_t$	Skewness	$\text{Skewness} = \frac{E\left[(x_t-\mu)^3\right]}{\sigma^3}$	FC	$\text{FC} = \frac{\sum_{k=1}^{K} f_k \cdot S(k)}{\sum_{k=1}^{K} S(k)}$	PF	$\text{SER} = \frac{E[(f_k-\text{FC})^4]}{\text{VF}^2}$
Std	$\sigma = \sqrt{\frac{1}{N}\sum_{t=1}^{N}(x_t-\mu)^2}$	Kurtosis	$K = \frac{E\left[(x_t-\mu)^4\right]}{\sigma^4}$	MSF	$\text{MSF} = \frac{\sum_{k=1}^{K} f_k^2 \cdot S(k)}{\sum_{k=1}^{K} S(k)}$	SER	$\text{PF} = \text{argmax}_f(A_k)$
RMS	$X_{\text{rms}} = \sqrt{\frac{1}{N}\sum_{t=1}^{N} x_t^2}$	Crest	$C_f = \frac{\max\|x_t\|}{X_{\text{rms}}}$	RMSF	$\text{RMSF} = \sqrt{\text{MSF}}$	/	/
Variance	$\sigma^2 = \frac{1}{N}\sum_{t=1}^{N}(x_t-\mu)^2$	Shape	$S_f = \frac{X_{\text{rms}}}{\frac{1}{N}\sum_{t=1}^{N}\|x_t\|}$	VF	$\text{VF} = \frac{\sum_{k=1}^{K}(f_k-\text{FC})^2 \cdot S(k)}{\sum_{k=1}^{K} S(k)}$	/	/
Peak	$X_{\text{peak}} = \max(\|x_t\|)$	Impulse	$I_f = \frac{X_{\text{peak}}}{\frac{1}{N}\sum_{t=1}^{N}\|x_t\|}$	RVF	$\text{RVF} = \sqrt{\text{VF}}$	/	/
SRA	$X_{\text{sra}} = \left(\frac{1}{N}\sum_{t=1}^{N}\sqrt{\|x_t\|}\right)^2$	Margin	$M_f = \frac{X_{\text{peak}}}{X_{\text{sra}}}$	SE	$\text{SE} = -\sum_{k=1}^{K} p_k \cdot \log(p_k)$	/	/

Considering that some redundant or weakly relevant indicators may interfere with the function approximation effect of the KAN model, this paper designs a multi-criteria evaluation mechanism to screen features. Using the Pearson correlation coefficient to measure the degree of association between each feature and the concrete vibration state, we then introduce variance analysis to quantify the information richness of each feature under different working conditions, thereby assessing its effectiveness as a classification criterion. Based on the comprehensive scores and a reasonable threshold, the top-performing core features are ultimately refined. This approach not only reduces data dimensionality while ensuring the model focuses on key physical features but also enhances the sensitivity of the system to hazardous operational signals, such as ground impacts and high-frequency idling, thereby laying a robust foundation for the equipment's active protection logic.

3.3.3. Data Normalization

In order to prevent differences brought by different physical dimensions from affecting the model training process, and to allow the loss function to converge faster, Min–Max normalization was applied to all input feature data, scaling them to the [0, 1] range:

$$x^* = \frac{x - x_{\min}}{x_{\max} - x_{\min}} \tag{9}$$

The normalization method eliminates differences in magnitude while fully preserving the original distribution of the signal itself, which is conducive to improving the numerical stability of the model during backpropagation.

3.4. Concrete Vibration State Recognition Algorithm Proposed in This Paper

To bridge the gap between construction quality control and active equipment protection, this paper proposes a hybrid recognition framework that leverages the feature extraction strength of CNNs and the precise nonlinear mapping of Kolmogorov–Arnold Networks (KAN). Considering that the sensor provides long-term signals, direct end-to-end learning in KAN could lead to computational overhead on edge nodes. Therefore, this framework utilizes a CNN front end to refine deep features, which are then processed by a KAN-based classification head to achieve millisecond-level decision-making. The overall structure is shown in Figure 6.

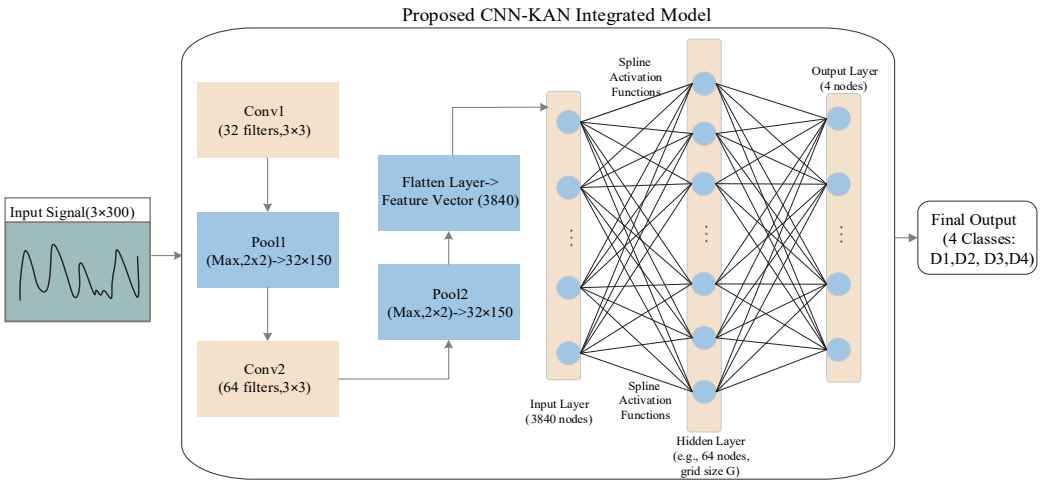


Figure 6. Overall architecture of the CNN-KAN for vibration signal classification.

The model abandons the traditional fully connected approach at the end of CNNs and instead incorporates a KAN module based on the Kolmogorov–Arnold representation theorem as the classification core. The CNN front end extracts deep feature vectors directly from raw vibration time-series signals through multilayer 1D convolution and pooling operations. The backend KAN module utilizes its internally learnable B-spline basis functions to perform curve connection and mapping on the deep features output by the CNN front end. Compared to traditional architectures, CNN_KAN employs learnable activation functions on the "edges," enabling a more detailed depiction of high-order nonlinear relationships within the data. This cascaded approach significantly reduces the number of model parameters while effectively improving the model's classification accuracy for working conditions with similar morphologies, such as "over-oscillation" and "dense" states.

To optimize the decision accuracy of multi-class classification tasks, this algorithm employs the cross-entropy loss function, whose mathematical expression is as follows:

$$\mathcal{L} = -\frac{1}{N}\sum_{i=1}^{N}\sum_{c=1}^{C} y_{i,c}\log(\hat{y}_{i,c}) \tag{10}$$

Here, N represents the number of samples, C represents the number of classes, Y is the one-hot encoding of the true labels, and P represents the predicted probability distribution of each class by the model. For parameter optimization, the Adam optimizer is used to ensure fast convergence. The final output of the CNN-KAN model is integrated into the equipment's control logic: when the predicted probability indicates a hazardous state (e.g., ground impact or idle vibration), the system triggers the industrial-grade alarm module immediately. This closed-loop design ensures that the equipment can autonomously mitigate mechanical wear while maintaining high-precision monitoring of the concrete vibration state.

4. Analysis of Experimental Results

4.1. Experimental Setup

To enable the experimental data to more accurately reflect the nonlinear variation characteristics of vibration signals in complex construction environments, all data collection for this study was conducted at actual concrete pouring sites. As shown in Figure 7, during the experiment, the high-precision wireless triaxial accelerometer was securely fastened to the end of the vibrator using straps. This installation method effectively prevents signal attenuation during transmission and ensures the sensor can move synchronously with the vibration source.



(**a**) (**b**)

Figure 7. Close-up of an accelerometer strapped to a vibrating rod. (**a**) Vibration in the air; (**b**) vibration in concrete.

Addressing the complex electromagnetic environment caused by high-density steel reinforcement mesh and high-power motors at construction sites, the experiment selected sensor nodes with strong anti-interference capabilities. For specific parameter configurations, please refer to Table 2.

Table 2. Parameter configuration.

Parameter	Value
Sampling Rate	200 Hz
Magnetic Fusion	Disabled
Accelerometer Filter	3
Gyroscope Filter	1
Magnetometer Filter	5
Static Threshold	5 dm
Static Zero Speed	255 cm/s

The sampling frequency was set to 200 Hz to balance signal fidelity with computational efficiency, ensuring that the embedded Raspberry Pi unit can acquire high-quality vibration data without causing buffer overflows. Beyond the hardware configuration, the software ecosystem of the intelligent system was implemented entirely in Python. Model training and evaluation were conducted using the PyTorch 2.2.2 and scikit-learn libraries. For hardware-level execution, the lgpio and spidev libraries were employed to manage sensor data acquisition, while PostgreSQL (via psycopg2) provided a robust local persistence layer for real-time data storage. The monitoring and feedback interface was constructed using the Flask and SocketIO frameworks to ensure low-latency data visualization and instantaneous acoustic alerting during the construction process.

4.2. Dataset Construction

4.2.1. State Definitions and Classifications

The data labeling standards for this experiment will strictly adhere to the physical evolution mechanisms of concrete vibration dynamics. To facilitate subsequent model input and result analysis, the experimental data are now categorized into the vibratory loading dataset DATASET1 and the no-load vibration dataset DATASET2 and provided symbolic definitions for the specific physical states under each set.

For the vibration operation condition dataset DATASET1, the logic for discrimination involves observing the envelope evolution of the signal amplitude and whether there are sudden changes in its frequency components. Define the idle reference state where the vibrator rod does not contact the concrete as D1. When the vibrator is inserted into the concrete, but the vibration time is insufficient, the signal amplitude is significantly suppressed due to strong dry friction between coarse aggregates. This under-vibrated condition is marked as D2. As the vibration continues, air bubbles are expelled from the concrete, and the slurry rises to the surface. When energy transfer efficiency reaches its optimal state, this degree of compaction is defined as D3. If the vibration time is too long, concrete segregation occurs, with aggregate settling reducing damping. The waveform exhibits low-damping, high-amplitude "liquefaction" oscillation characteristics. This over-damped state is classified as D4.

For the DATASET2 of empty vibration conditions, classification is based on the characteristics of the acceleration vector distribution derived from Newton's Second Law. When the vibrator is placed horizontally, the acceleration due to the vertical component of gravity (Y-axis) approaches zero. This horizontal no-load vibration condition is denoted as F1. When the vibrator is suspended vertically, the signal exhibits periodic sinusoidal oscillations dominated by gravity. This vertical free-vibration state is denoted as F2. When the vibrator head intermittently strikes the ground, the instantaneous bearing capacity and rigid collision of the ground cause the signal to contain numerous non-steady spike pulses, with amplitude fluctuating violently. This ground-contact and no-load vibration state is denoted as F3.

This study first anchors the effective time intervals for each state based on the previously mentioned dynamic characteristics. Subsequently, a continuous stable waveform segment of 2 s in length (totaling 800 sampling points) is extracted to serve as the raw physical baseline for subsequent model training.

4.2.2. Construction of Time-Series Datasets

To accommodate the input requirements of CNN and CNN-KAN models and overcome the issue of overfitting on small samples, the experiment employed sliding window technology to augment the benchmark data. The experiment was set with a window width of 300 samples and a sliding step size of five samples for cyclic sampling. This process constructs raw time-series datasets directly applicable for deep learning model training. The details of the sample distribution are shown in Table 3.

Table 3. Category definitions and sample distribution of experimental datasets.

Dataset Type	Status Tab	Sample Size	Window Size	Sampling Frequency
DATASET1	D1	100	300	200 Hz
	D2	100	300	200 Hz
	D3	100	300	200 Hz
	D4	100	300	200 Hz
DATASET2	F1	100	300	200 Hz
	F2	100	300	200 Hz
	F3	100	300	200 Hz

4.2.3. Feature Set Construction

In the comparative experiment, the KAN model cannot directly process the raw triaxial time-series signals due to its network architecture. Therefore, this study performed feature transformation on the samples obtained through sliding window sampling. First, feature extraction is performed on the original signal in both the time domain and the frequency domain. A preliminary feature pool comprising 20 initial features, including variance, root mean square value, peak factor, and energy in specific frequency bands, has been established. The specific names and mathematical definitions of the indicators are detailed in Table 1. To quantify the representational capability of each feature for different operating conditions and optimize computational efficiency, a dual quantitative assessment of characteristic efficacy was conducted using Pearson's correlation coefficient and analysis of variance.

During the specific screening process, the study conducted a quantitative analysis of the performance of each feature across two independent recognition tasks. Taking the task of identifying vibration states as an example, Figure 8 shows the comprehensive correlation score ranking between the initial features and the four states of concrete. From the distribution pattern of the data in the figure, it can be observed that the root mean square value and skewness demonstrate distinct advantages in characterizing signal energy evolution and waveform asymmetry. These indicators, positioned at the top of the scoring table, have become key physical criteria for distinguishing between conditions with particularly similar physical characteristics, such as dense compaction and overcompaction.

For the task of identifying types of no-load vibration, Figure 9 completely documents the specific process of feature selection and the distribution characteristics of scores. When processing touchdown signals with transient impacts, frequency-domain metrics such as frequency center of gravity prove to be of paramount importance, carrying extremely high discriminative weight. This indicates that the metric can sensitively capture spectral fluctuations caused by random collisions. Thus, from a dynamic perspective, this provides crucial support for the detailed classification of complex no-load vibration states.

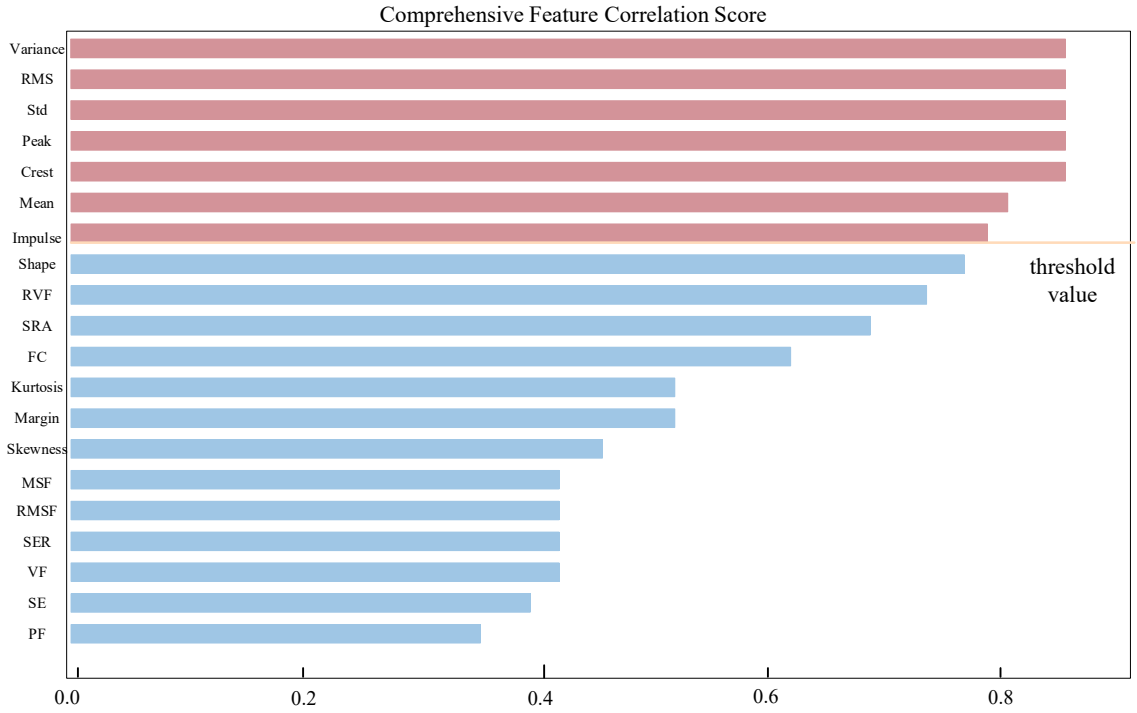


Figure 8. Comprehensive correlation score ranking of features for concrete vibration state classification (DATASET1).

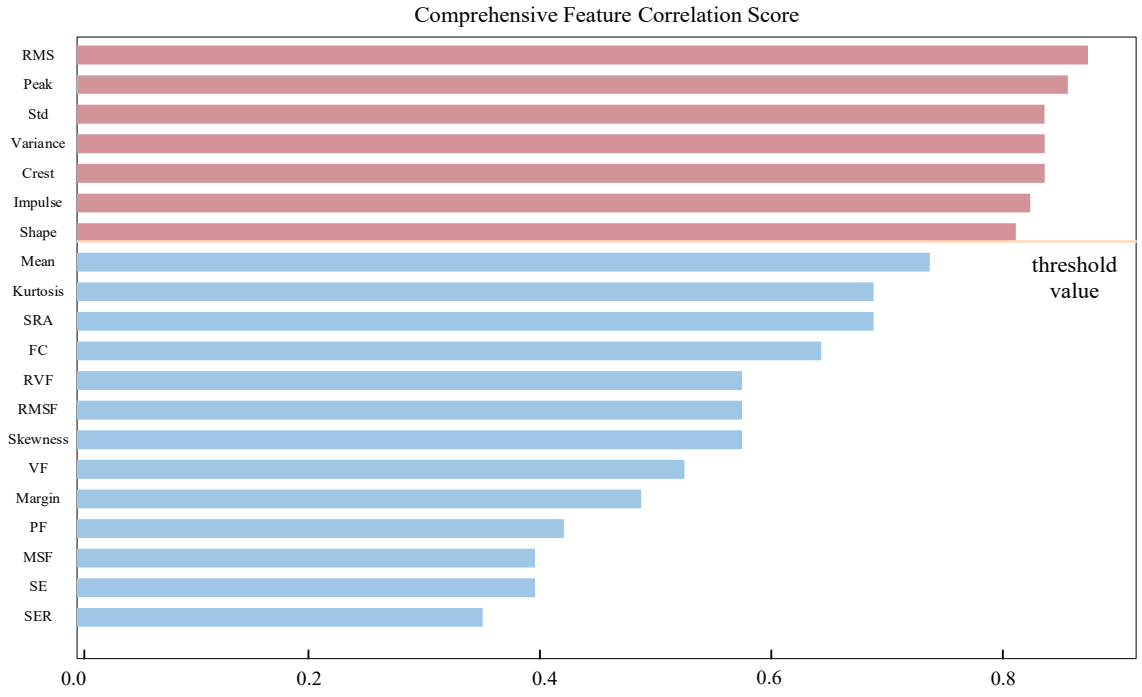


Figure 9. Comprehensive correlation score ranking of features for no-load vibration type classification (DATASET2).

By comparison, it can be seen that despite minor differences between tasks, core metrics such as root mean square value, skewness, and frequency center of gravity all exhibit high discriminative weights across both task categories. Based on these results, the experiment ultimately selected seven of the most representative core features from the initial 20 indicators to form the input vector. This operation reduces the feature dimension

by 65% while preserving over 95% of the critical physical information, thereby constructing a feature dataset specifically tailored for KAN model training, as detailed in Table 4.

Table 4. Feature datasets.

Dataset Type	Status Tab	Sample Size	Input Dimension
DATASET1	D1	100	7×1
	D2	100	7×1
	D3	100	7×1
	D4	100	7×1
DATASET2	F1	100	7×1
	F2	100	7×1
	F3	100	7×1

4.3. Evaluation Criteria

To quantitatively evaluate the performance of the CNN-KAN model in concrete vibration state recognition across multiple dimensions, this paper selects accuracy, precision, recall, and F1-score as core evaluation metrics. These metrics collectively form a comprehensive evaluation framework that assesses the model's overall performance, prediction accuracy, classification completeness, and robustness under category imbalance. The relevant performance evaluation metrics and their mathematical expressions are as follows:

$$\text{Accuracy} = \frac{TP + TN}{TP + TN + FP + FN} \tag{11}$$

$$\text{Precision} = \frac{TP}{TP + FP} \tag{12}$$

$$\text{Recall} = \frac{TP}{TP + FN} \tag{13}$$

$$F_1\text{−score} = 2 \times \frac{\text{Precision} \times \text{Recall}}{\text{Precision} + \text{Recall}} \tag{14}$$

where TP, TN, FP, and FN denote the numbers of true positives, true negatives, false positives, and false negatives, respectively.

The accuracy metric measures the proportion of correct predictions made by the model across the entire dataset. Precision focuses on quantifying the proportion of true positives among samples predicted as positive, thereby reflecting the accuracy of the model's decision-making. Recall focuses on the proportion of true positives that are correctly retrieved, serving as a measure of the system's identification coverage capability. Considering that data from construction sites may exhibit characteristics of uneven category distribution, this paper introduces the F1-score as the harmonic mean of precision and recall to comprehensively evaluate a model's classification robustness under complex operating conditions.

In addition to the quantitative indicators mentioned above, this experiment also incorporates multiple visualizations for in-depth analysis. The experiment uses ROC curves to depict the relationship between true positive rate and false positive rate at different thresholds, serving to evaluate the model's overall classification performance. The confusion matrix visually illustrates the misclassification patterns across different categories. Additionally, experiments can compare the convergence speed, training stability, and potential overfitting risks of different algorithmic architectures by examining the variation in loss functions and accuracy rates.

In the evaluation process, all experimental training data are divided into training and test sets according to established standards to ensure the objectivity and comparability of experimental results under equivalent benchmarks.

4.4. Comparative Experiment

To systematically validate the performance of the CNN-KAN model, comparative experiments were conducted on two independent datasets: a vibration test dataset and a no-load vibration test dataset. The experiment conducts a comparative evaluation of the proposed CNN-KAN against CNN and KAN. The following sections will detail model configurations, data characteristics, and specific recognition results across different experimental scenarios.

4.4.1. Concrete Vibration Condition Test

The core objective of this experiment is to verify whether the proposed model can accurately identify the four key states of concrete vibration compaction: empty vibration, under-vibration, vibration compaction, and over-vibration. For this task, this paper constructs the corresponding comparison sequences. The specific parameter configurations and hyperparameter settings for each model are shown in Table 5.

Table 5. Model structure and hyperparameter configuration for vibration type dataset.

Category	Parameter	Baseline CNN	Baseline KAN	CNN-KAN (Proposed)
Input and Architecture	Input Data Format	Raw 1D Signal (1 × 300)	Statistical Feature (7 × 1)	Raw 1D Signal (1 × 300)
	Convolutional Layer 1	Conv (k = 3, s = 1, p = 2) 13 filters	—	Conv (k = 4, s = 1, p = 1), 13 filters
	Pooling 1	BN, Max Pool (k = 3)	—	BN, Max Pool (k = 2)
	Convolutional Layer 2	Conv (k = 3, s = 1, p = 2) 17 filters	—	Conv (k = 3, s = 1, p = 1), 23 filters
	Pooling 2	BN, Max Pool (k = 2)	—	BN, Max Pool (k = 2)
	Dimension Reduction	Global Average Pooling	—	Global Average Pooling
	Classifier Head	Fully Connected: [17 → 4]	KAN:[7,3,4,4]	KAN:[23 → 4]
	KAN Parameters	—	grid = 3, spline = 1	grid = 5, spline = 1
Training Config	Optimizer	Adam	Adam	Adam
	Loss	Cross Entropy	Cross Entropy	Cross Entropy
	Learning Rate	0.00085	0.02	0.00085
	Training Epochs	300	300	300

Based on the configuration scheme, the three models exhibit distinct mapping logic when processing vibration signals. The CNN module employs convolution operators to achieve hierarchical dimensionality reduction in the original sequence and capture local features. The KAN module leverages the approximation advantages of B-spline functions to decouple complex high-order nonlinear relationships within the feature space. Given this situation, CNN-KAN employs a tandem coupling approach to construct a classification system that progresses from automatic feature refinement to nonlinear discrimination.

The raw vibration waveforms for each vibration state are shown in Figure 10. The evolution of the raw vibration waveform across four states can be clearly observed: from the regular oscillations of the empty state D1, to the suppressed low amplitude of the under-vibrated state D2, then to the enhanced energy of the compacted state D3, and finally to the high-frequency oscillations of the over-vibrated state D4. The core challenge lies in the fact that the waveforms of dense D3 and over-vibrated D4 appear remarkably similar in later stages, like twins, making it easy for traditional simple classification methods to misidentify them. The proposed CNN-KAN architecture utilizes front-end convolutional layers to extract local features, combined with the B-spline fitting capability of the back-end KAN, effectively capturing minute damping and frequency variations. This overcomes the bottleneck where linear classifiers struggle to distinguish subtle differences.

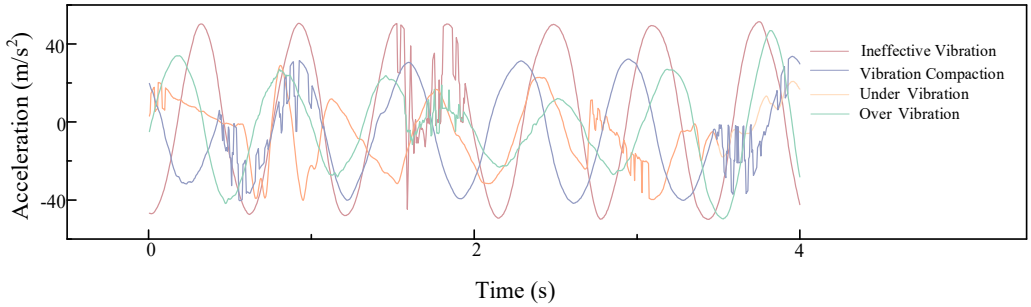


Figure 10. Representative time-domain signal segments of the vibration type dataset.

This design advantage is particularly evident in the model's convergence. As shown in the training and testing loss curves recorded in Figure 11, the CNN-KAN model exhibited a significant decline in loss values within the first 10 epochs and quickly stabilized at a low level. Its convergence trajectory markedly outperforms both the descent path of traditional CNN and the slow convergence of KAN.

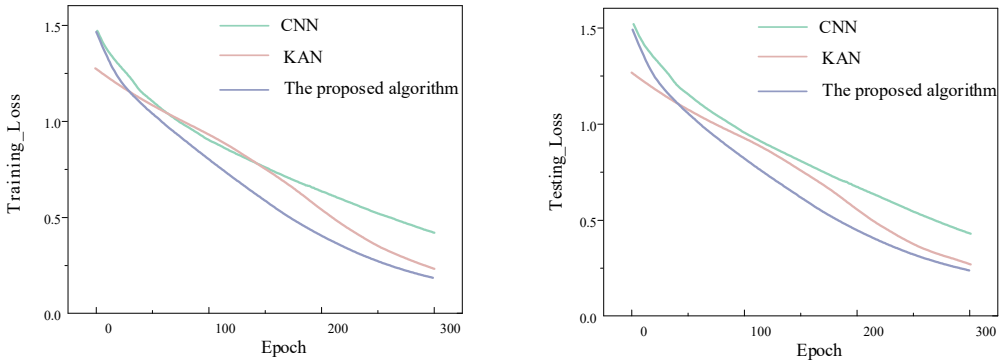


Figure 11. Convergence curves of different models on the vibration type dataset.

The trend in test set accuracy over iterations further supports the above conclusion, as shown in Figure 12. Although the baseline CNN achieves high accuracy, its curve exhibits a step-like ascent accompanied by persistent fluctuations in the 0–50 epoch range, and its corresponding loss curve descends significantly slower than that of CNN-KAN. Such instability indicates that the traditional CNN is highly sensitive to parameter settings, primarily due to the high parameter density in its fully connected layers, which complicates gradient convergence when processing non-stationary vibration signals. The learning rate of the KAN model, however, lags behind. In contrast, the CNN-KAN model demonstrates superior learning efficiency from the outset of training, rapidly surpassing the 90% accuracy threshold while maintaining stable performance because the learnable B-spline functions on the edges of the KAN module achieve smoother local fitting and faster optimization. This "fast convergence, high retention" characteristic means that in practical engineering applications, the model can significantly reduce training time costs while demonstrating greater robustness to data perturbations.

To verify the model's reliability under random conditions, Figure 13 shows the accuracy distribution from ten independent replicate experiments. Unlike the relatively divergent distribution characteristics of the CNN and KAN models, the experimental results of the CNN-KAN model exhibit high concentration, presenting a sharp peak morphology with significantly compressed standard deviation. This extremely low result dispersion indicates that the hybrid architecture effectively counteracts the uncertainty introduced by random initialization through complementary advantages, ensuring high reproducibility of the algorithm in non-stationary construction signal processing.

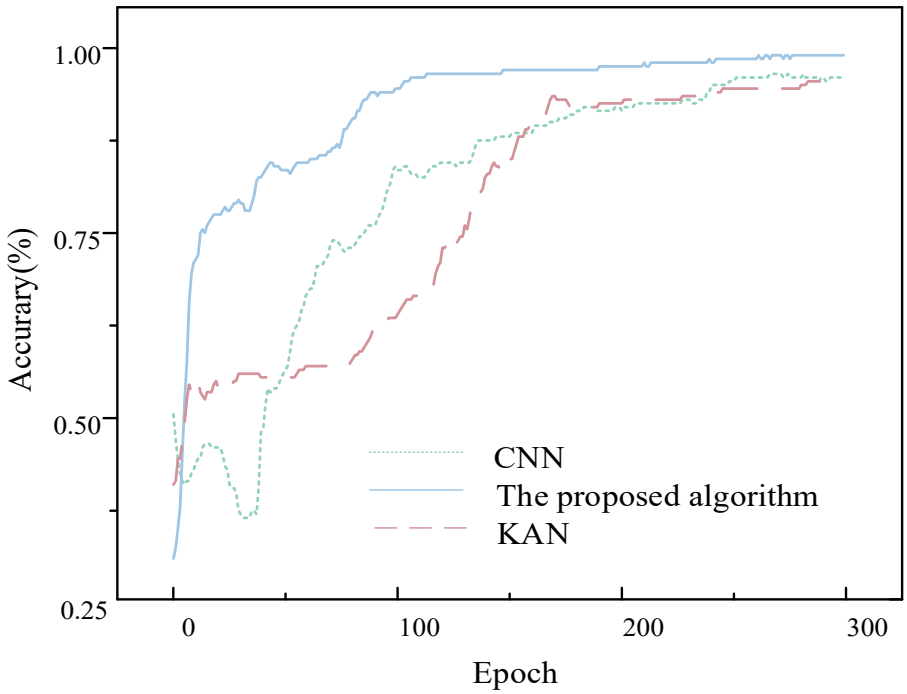


Figure 12. Accuracy comparison of different models on the vibration type dataset.

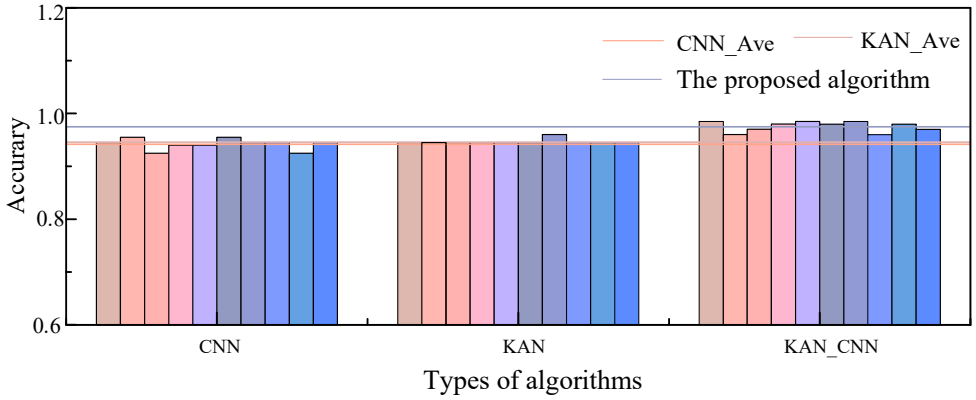


Figure 13. Histogram of accuracy over ten repeated experiments for the vibration type dataset.

Figure 14 illustrates the detailed classification performance of the three models on the test set. Comparing the probability distributions of predictions across different categories, it reveals the decision-making differences among different architectures when handling hard-to-classify samples.

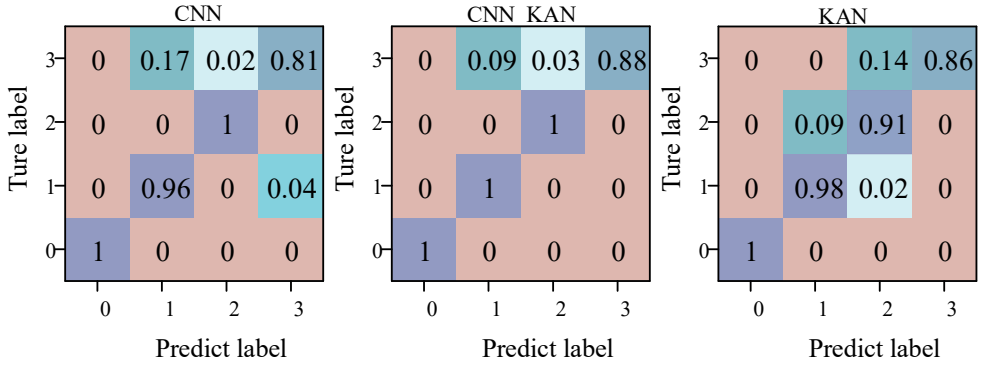


Figure 14. Confusion matrix of the KAN-CNN model on the vibration type dataset.

The CNN model on the left achieved perfect classification for labels 0 and 2, but encountered a significant bottleneck in recognizing label 3, with a prediction accuracy of only 81%. It is worth noting that the CNN model exhibits specific structural misclassifications, incorrectly categorizing 17% of label 3 samples as label 1. Physically, this stems from the fact that over-vibration (label 3) and compacted (label 2) states exhibit extremely high similarity in vibration waveforms during the late stages of liquefaction, functioning as "twin signals". This cross-category misclassification highlights an issue where traditional convolutional networks experience feature aliasing when capturing these subtle damping offsets and frequency drifts, making it difficult to precisely distinguish the physical differences between non-adjacent operating conditions. The KAN model on the right exhibits a completely different pattern of misclassification, with its primary errors concentrated between adjacent categories. Although the model performs relatively stably on label 0, it exhibits significant classification ambiguity across the intermediate categories. The CNN-KAN model demonstrates superior discriminative power, particularly in distinguishing between "compacted" (label 2) and "over-vibrated" (label 3) states. By utilizing the learnable B-spline basis functions within the KAN module to accurately disentangle high-order nonlinear features, the hybrid architecture effectively resolves overlapping feature boundaries that traditional networks overlook. The significant reduction in misclassification compared to baseline models confirms that the hybrid architecture can effectively capture the subtle damping shifts required for autonomous construction quality control.

The classification performance is demonstrated by the ROC curve in Figure 15. The curve of the CNN-KAN model rapidly approaches the ideal inflection point in each category, with values approaching one infinitely. This near-perfect data not only demonstrates the model's high discriminative power in feature space but also indicates its ability to adapt to the diverse and complex conditions found in construction environments. Compared to models with more common feature overlap regions, it exhibits significantly greater potential for engineering applications.

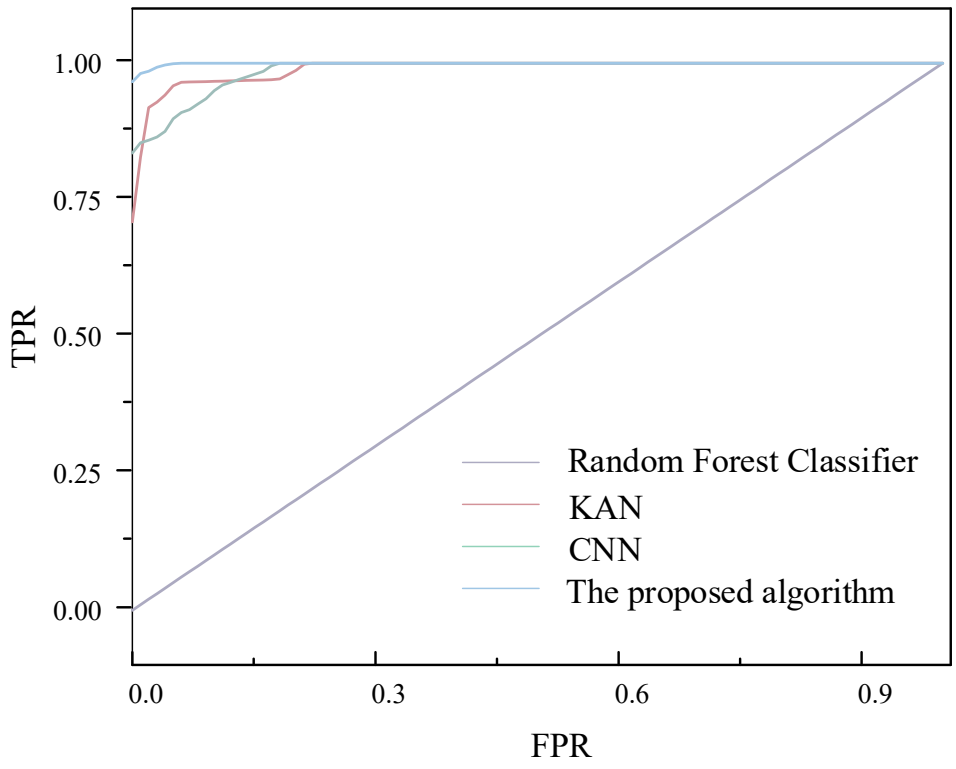


Figure 15. ROC curves for each class using the KAN-CNN model on the vibration type dataset.

4.4.2. Experimental Investigation of the Internal Vibrator Under No-Load Conditions

This experiment primarily focuses on three common abnormal operating conditions: horizontal no-load vibration, vertical no-load vibration, and ground-contact no-load vibration. It aims to verify whether the model can accurately make judgments when confronted with unstable impact signals. Considering that no-load vibration signals may contain transient pulses, the experiment implemented targeted measures in the model structure. The specific parameter configurations are shown in Table 6.

Table 6. Model structure and hyperparameter configuration for the no-load vibration type dataset.

Category	Parameter	Baseline CNN	Baseline KAN	CNN-KAN (Proposed)
Input and Architecture	Input Data Format	Raw 1D Signal (1 × 300)	Statistical Feature (7 × 1)	Raw 1D Signal (1 × 300)
	Convolutional Layer 1	Conv (k = 2, s = 1, p = 2) 13 filters	—	Conv (k = 2, s = 1, p = 1), 13 filters
	Pooling 1	BN, Max Pool (k = 2)	—	BN, Max Pool (k = 2)
	Convolutional Layer 2	Conv (k = 1, s = 1, p = 2) 17 filters	—	Conv (k = 1, s = 1, p = 1), 23 filters
	Pooling 2	BN, Max Pool (k = 2)	—	BN, Max Pool (k = 2)
	Dimension Reduction	Global Average Pooling	—	Global Average Pooling
	Classifier Head	Fully Connected: [17 → 3]	KAN:[7,3,4,3]	KAN:[23 → 3]
	KAN Parameters	—	grid = 3, spline = 1	grid = 5, spline = 1
Training Config	Optimizer	Adam	Adam	Adam
	Loss	Cross Entropy	Cross Entropy	Cross Entropy
	Learning Rate	0.0008	0.00055	0.00055
	Training Epochs	300	300	300

The baseline CNN model retains the standard two-layer small-kernel convolution architecture (with kernel size three and stride one), placing greater emphasis on preserving the temporal information of the original signal. In contrast, the proposed CNN-KAN architecture adopts a down-sampling convolution strategy with a stride of two, combined with max-pooling layers to achieve greater feature compression. The design aims to leverage the dimensionality reduction effect of convolutional layers in the temporal dimension to isolate high-frequency touchdown collision signals from redundant information. These signals are then fed into a 4000-dimensional input KAN for end-to-end nonlinear discrimination, thereby enhancing the system's ability to identify high-frequency abrupt changes within touchdown signals.

Figure 16 clearly shows that the three types of no-load vibration states exhibit distinct differences in their time-domain waveforms. In the horizontal free-vibration state, due to the equilibrium of forces, only a small-amplitude steady background noise is observed along the Y-axis. Vertical no-load vibration is primarily influenced by gravity, with the waveform exhibiting regular sinusoidal oscillations. Ground-contact vibration is far more complex. Due to high-frequency, random collisions between the rod tip and the ground, the waveform contains numerous unstable spike pulses and abrupt energy fluctuations. When confronted with complex signals featuring transient impacts, the CNN-KAN architecture demonstrates exceptional adaptability. Its front-end down-sampling convolutional layer effectively captures the transient high-frequency features generated by collisions, while the rear-end KAN utilizes nonlinear mapping to analyze the dynamic sudden change patterns embedded within the waveform.

In terms of training dynamics, Figure 17 records the descent trajectories of different models on the loss function. Experimental observations reveal that when processing raw signals containing transient impacts, the KAN model exhibits persistent numerical fluctuations in its loss curve during descent due to its lack of preprocessing capability for high-frequency features. Furthermore, its convergence speed is significantly constrained.

In contrast, the CNN-KAN loss curve exhibits excellent overall smoothness and shows no signs of oscillation. This convergence advantage demonstrates that the front-end CNN module in the hybrid architecture effectively acts as a filter, eliminating redundant noise generated by ground-contact collisions. This provides the back-end KAN component with feature inputs characterized by a high signal-to-noise ratio and strong discriminative power, ensuring a stable and efficient gradient descent process.

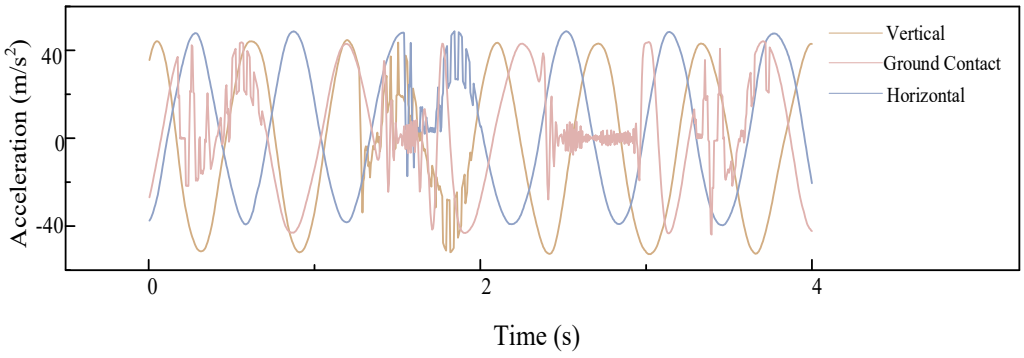


Figure 16. Representative time-domain signal segments of the no-load vibration type dataset.

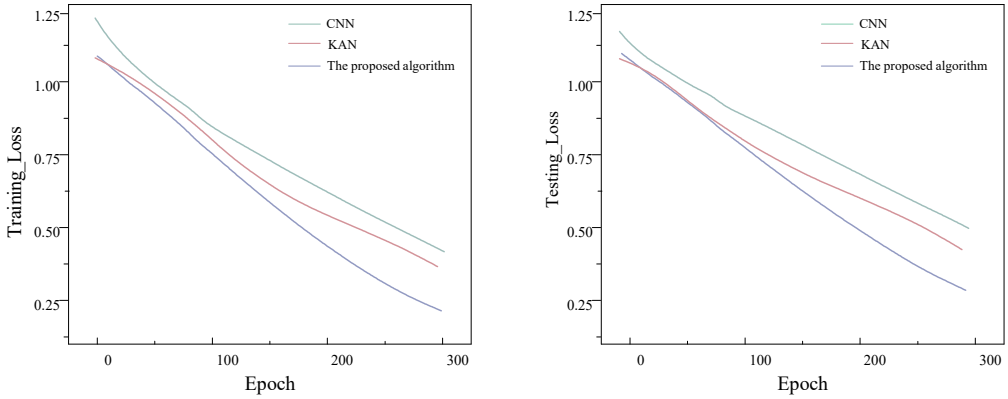


Figure 17. Convergence curves of different models on the no-load vibration type dataset.

The curve showing the change in test accuracy over training iterations is depicted in Figure 18. The CNN-KAN model demonstrates rapid learning capabilities, with its performance curve climbing steeply within a short number of epochs before stabilizing at a plateau. The overall trajectory is compact and steady. In contrast, other comparison models exhibit relatively sluggish upward trajectories, and even during the stabilization phase, they inevitably experience varying degrees of fluctuation. This "fast and stable" learning characteristic precisely demonstrates that hybrid architectures indeed offer advantages in feature extraction efficiency. It can quickly identify key factors within non-stationary signals, significantly reducing the training cycles required to achieve optimal model performance.

To further quantify the model's generalization stability under random disturbances, Figure 19 shows the accuracy distribution across ten independent replicate experiments. The relatively broad distribution range of the CNN and KAN models indicates that their performance is significantly influenced by parameter initialization. In contrast, the accuracy distribution histogram of CNN-KAN exhibits the narrowest and most concentrated distribution. This extremely low variance characteristic effectively demonstrates the robustness of the hybrid architecture. Even when confronted with pulse signals exhibiting random characteristics, the model consistently delivers highly consistent classification results, demonstrating strong engineering reproducibility.

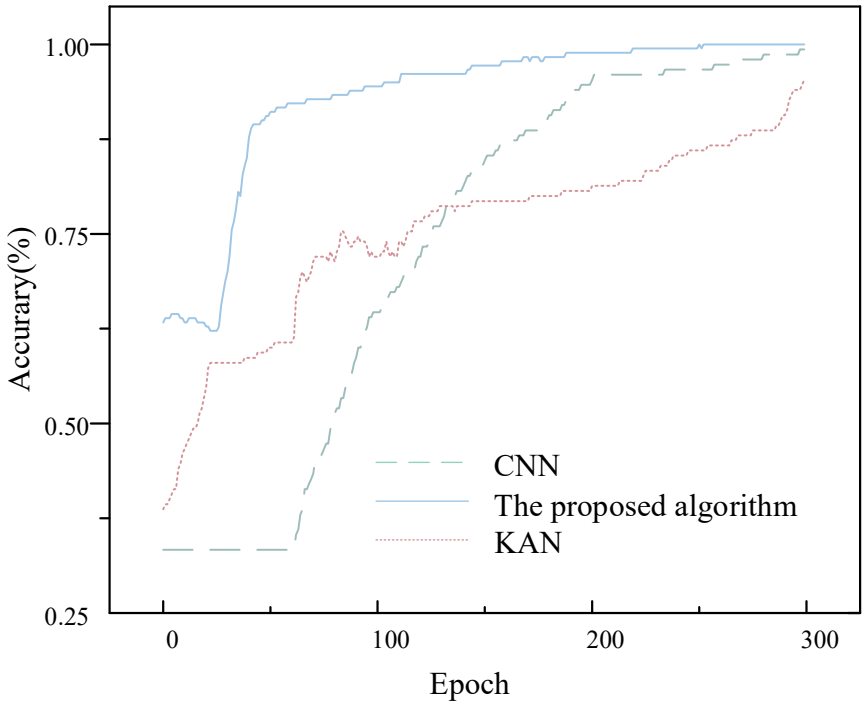


Figure 18. Accuracy comparison of different models on the no-load vibration type dataset.

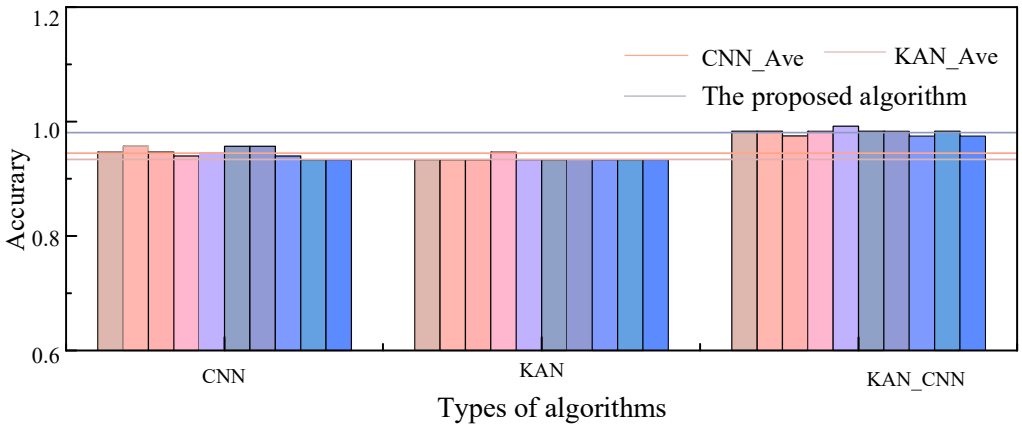


Figure 19. Histogram of accuracy over ten repeated experiments for the no-load vibration type dataset.

Figure 20 reveals the model's exceptional performance in identifying "ground impact" (label 2), achieving near-perfect accuracy. From the perspective of equipment protection, this capability allows the intelligent system to detect high-energy collision pulses instantaneously. Unlike the baseline CNN and KAN models, which exhibit blurred decision boundaries for transient impacts, CNN-KAN effectively filters out redundant noise, ensuring that the active protection mechanism triggers the alarm only during genuine hazardous conditions. This high sensitivity to impact signals is fundamental to extending the service life of the vibrating rod in chaotic construction sites.

Figure 21 further quantifies the classification performance of each model at different thresholds using ROC curves. By observing the curve shapes, the CNN-KAN model exhibits steep, near-vertical ascents across all categories, rapidly converging toward the ideal classification point in the upper-left corner. This demonstrates that the model can maintain an exceptionally high true positive rate while simultaneously suppressing the false positive rate to near zero. Compared to it, the curves of the CNN and KAN models appear slightly flatter at the inflection points, indicating that there remains a certain margin of uncertainty for samples with lower confidence levels. Numerical analysis indicates that

CNN-KAN achieves AUC values approaching one across all categories. This near-perfect figure reaffirms the advantages of the model's feature extraction and nonlinear mapping capabilities. This model not only addresses the shortcomings of a single model in a specific category but also constructs a decision space with strong discriminative capabilities across the entire range. This ensures that in complex and dynamic construction site environments, both regular periodic vibrations and random impact signals can be accurately identified and separated.

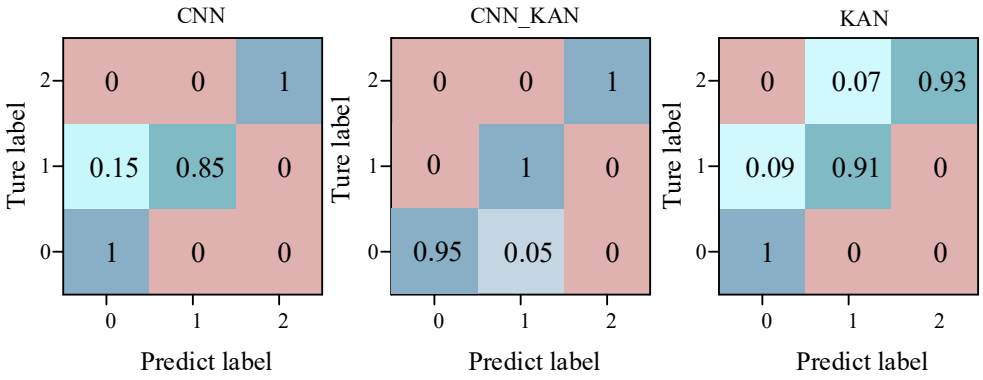


Figure 20. Confusion matrix on the no-load vibration type dataset.

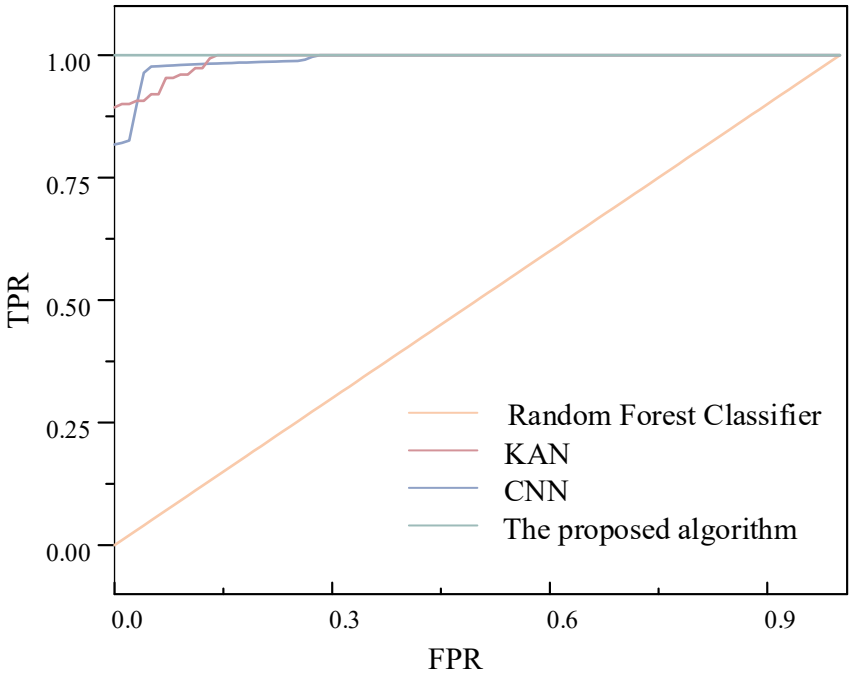


Figure 21. ROC curves for each class using the KAN-CNN model on the no-load vibration type dataset.

The experimental results validate that CNN-KAN achieves a synergistic balance between feature refinement and efficient mapping, demonstrating superior performance in identifying transitional states with blurred physical boundaries. The significant advantage of this hybrid architecture lies in its high parameter efficiency and high-order nonlinear fitting capability, which allows the model to maintain elevated recognition precision even under the strict computational constraints of low-power edge nodes. Consequently, this framework is particularly well-suited for the intelligent upgrading of construction machinery where millisecond-level response and high-fidelity monitoring are required. Its robustness to data perturbations and fast convergence properties provide a

reliable technical roadmap for real-time automated construction quality control in complex site environments.

4.5. Discussion

Combining the experimental results from both datasets, CNN-KAN outperforms the single model across all performance metrics. As shown in Table 7, this model outperforms the single model in terms of recognition accuracy, precision, recall, and F1-score, demonstrating exceptional robustness and classification stability.

Table 7. Comparison of performance metrics across different models.

Dataset	Model	Accuracy	Precision	Recall	F1-Score
Vibration Types	CNN	0.9420 ± 1.03%	0.9276	0.9256	0.9256
	KAN	0.9465 ± 0.47%	0.9434	0.9411	0.9459
	CNN_KAN	0.9755 ± 0.98%	0.9800	0.9797	0.9809
No-load Types	CNN	0.9456 ± 0.90%	0.9358	0.9358	0.9444
	KAN	0.9346 ± 0.42%	0.9415	0.9377	0.9444
	CNN_KAN	0.9817 ± 0.53%	0.9848	0.9838	0.9837

In the vibration type identification task, the CNN-KAN model achieved a test accuracy of 97.55%, representing a 3.35 percentage point improvement over the pure CNN model. Its core highlight lies in the structural design that effectively integrates the hierarchical feature extraction capability of CNN with the precise nonlinear mapping capability of KAN. In actual working conditions, the waveforms of "over-vibration" and "vibration compaction" in concrete appear remarkably similar, and traditional models often struggle to capture the subtle nonlinear differences between them. CNN-KAN leverages B-spline functions that can be learned from adjacent data points to more precisely capture damping shifts caused by varying degrees of concrete liquefaction. This enables it to demonstrate superior discrimination capabilities in conditions prone to confusion.

In terms of identifying the no-load condition, the model achieved an optimal accuracy of 98.17%. The standard deviation across multiple experiments was only ±0.53%, demonstrating the model's high consistency and reliability. From experimental analysis, the KAN model demonstrates superior approximation capabilities for small-scale high-dimensional features. However, when confronted with raw features not processed through deep CNN layers, its noise robustness is slightly inferior to that of hybrid architectures.

The experimental results validate that CNN-KAN achieves a synergistic balance between feature refinement and efficient mapping. This tandem architecture enables the equipment to maintain high-precision monitoring under variable loads while responding to sudden pulses (such as ground strikes) with consistent reliability (standard deviation of ±0.53%). Overall, this research provides a viable technical pathway for a new generation of intelligent construction tools that possess both "construction state awareness" and "self-protection capabilities," optimized for high-performance execution on low-power embedded devices. From an industrial feasibility perspective, the estimated hardware cost of this smart integrated module is approximately 800 RMB, which facilitates large-scale deployment on standard vibratory machinery. Field evaluations indicate that by reducing human judgment errors, the implementation of this real-time monitoring and warning system can significantly improve the construction process acceptance rate (compaction qualification rate) in laboratory settings. Furthermore, the Raspberry Pi 5 platform offers substantial hardware expandability through its GPIO and RS485 interfaces. Future development will focus on integrating the system with a variable-frequency drive (VFD) to establish a complete active vibration control mode. In this closed-loop control configuration, the equipment will be able to autonomously adjust the motor's vibration frequency according

to the identified liquefaction stage, achieving a transition from a pure diagnostic tool to an autonomous process regulator.

5. Conclusions

This study developed an intelligent vibration system built on an edge computing architecture and proposed a CNN-KAN fusion framework for recognizing vibration states. The model was meticulously crafted to simultaneously tackle two pragmatic challenges: the assessment of concrete compaction quality during construction activities and the facilitation of the equipment's ability to autonomously identify its anomalous operational conditions. The principal findings are delineated as follows:

(1) The CNN-KAN model attained a test accuracy of 97.55% in the classification of vibration states. The implementation of convolutional neural networks for dimensionality reduction and feature extraction prior to the data being input into the KAN module significantly alleviated the computational burden and circumvented the convergence issues that KAN typically experiences with extensive time-series data. The findings substantiate that the amalgamation of deep feature extraction with KAN-based nonlinear classification is proficient for the differentiation of intricate physical signals.

(2) On the no-load vibration dataset, which contains transient impact components, the model reached a recognition accuracy of 98.17%, with a standard deviation of $\pm 0.53\%$ across ten independent runs. The model correctly separated regular cyclic signals, such as vertical no-load responses, from signals with random impulsive content, such as ground-contact vibrations. The minimal variance observed across the runs reflects a consistent and stable performance, indicating an insensitivity to initial conditions.

(3) Serving as an exploratory application in the domain of concrete vibration quality monitoring, the CNN-KAN framework provides elevated classification accuracy while preserving a compact architecture and rapid convergence. This equilibrium renders it exceptionally suitable for implementation on embedded systems with limited computational capabilities, where both precision and efficiency are paramount for real-time automated monitoring in construction environments.

(4) Future work will prioritize the correlation between real-time vibration states and the 28-day compressive strength of concrete specimens through a series of destructive tests. This will provide a quantitative baseline for establishing the relationship between vibration energy and structural performance. Additionally, porting the proposed CNN-KAN framework to ultra-low-power microcontrollers such as the ESP32 will be investigated to further reduce system costs and enhance energy efficiency for specific industrial scenarios. These advancements aim to bridge the gap between theoretical algorithm design and large-scale industrial applications in smart construction toolchains.

Author Contributions: Conceptualization, T.W. and X.W.; methodology, T.W. and S.H.; software, T.W. and T.X.; validation, S.H., Z.C. and M.M.S.; formal analysis, S.H. and T.X.; investigation, Z.C. and S.Y.; resources, S.Y., X.W. and B.F.; data curation, S.Y. and M.M.S.; writing—original draft preparation, T.W. and Z.C.; writing—review and editing, X.W., S.Y., B.F. and M.M.S.; visualization, Z.C. and T.X.; supervision, X.W. and S.Y.; project administration, X.W.; funding acquisition, X.W. and S.Y. All authors have read and agreed to the published version of the manuscript.

Funding: This work was funded by "Key Scientific Research Projects of Colleges and Universities in Henan province, grant number 26A560013", and "Key R&D and Promotion Projects in Henan Province, grant number 262102320052". and "the Science and Technology Research and Development Project of China Construction Sixth Engineering Bureau Corp., Ltd., grant number CSCEC6B-2024-Z-4 and

CSCEC6B-2025-Z-4", and "the Science and Technology Research and Development Project of China State Construction Engineering Corporation, Ltd., grant number CSCEC-2023-Z-19 and CSCEC-2025-Z-20".

Data Availability Statement: The datasets presented in this article are not readily available due to technical and time limitations. Requests to access the datasets should be directed to wangxinwei@ncwu.edu.cn.

Acknowledgments: The authors would like to express their sincere gratitude to Shang Chao, Peng Yujia, Qian Chao, Zha Pinwang, and Chen Shanke for their invaluable assistance during the experimental phase of this study. Their unremitting efforts in establishing vibration testing devices, assisting in data collection processes, and preparing concrete samples have played an important role in the successful validation of intelligent vibration machines.

Conflicts of Interest: Authors Tianlong Wang and Zhaohui Cai were employed by the company CSCEC City Construction Development Co., Ltd. The remaining authors declare that the research was conducted in the absence of any commercial or financial relationships that could be construed as a potential conflict of interest.

References

1. Shin, T.Y.; Kim, J.H. Flow simulation of fresh concrete accounting for vibrating compaction. *Cem. Concr. Res.* **2023**, *173*, 107300. [CrossRef]
2. Jiang, D.Q.; Kong, L.J.; Wang, H.; Pan, D.; Li, T.; Tan, J. Precise control mode for concrete vibration time based on attention-enhanced machine vision. *Autom. Constr.* **2024**, *158*, 105221. [CrossRef]
3. Yang, Y.; Zhao, W.G. Analysis on identifying thin-plate void parameters in concrete based on vibro-acoustic method. *Measurement* **2025**, *242*, 116281. [CrossRef]
4. Yang, F.; Yao, Y.S.; Wei, J.; Wang, X.X.; Feng, Z.X. Estimating the effect of vibration mixing process on air pore size distributions in concrete using digital image analysis. *Buildings* **2022**, *12*, 1142. [CrossRef]
5. Zheng, Y.Z.; Zhou, Y.; Nie, F.; Luo, H.Y.; Huang, X.M. Effect of a novel vibration mixing on the fiber distribution and mechanical properties of ultra-high performance concrete. *Sustainability* **2022**, *14*, 7920. [CrossRef]
6. Cavalaglio Camargo Molano, J.; Rubini, R.; Cocconcelli, M. Experimental evidence of the speed variation effect on SVM accuracy for diagnostics of ball bearings. *Machines* **2018**, *6*, 48. [CrossRef]
7. Ye, G.T.; Qu, J.S.; Tao, J.T.; Dai, W.; Mao, Y.F.; Jin, Q. Autonomous surface crack identification of concrete structures based on the YOLOv7 algorithm. *J. Build. Eng.* **2023**, *73*, 106688. [CrossRef]
8. Huang, S.H.; Wang, T.G.; Zeng, G.F. Deep learning-based method for damage identification and localization of the maglev track stator surface. *High-Speed Railw.* **2026**, *4*, 21–26. [CrossRef]
9. Bai, Z.L.; Liu, T.J.; Zou, D.J.; Zhang, M.; Zhou, A.; Li, Y. Image-based reinforced concrete component mechanical damage recognition and structural safety rapid assessment using deep learning with frequency information. *Autom. Constr.* **2023**, *150*, 104839. [CrossRef]
10. Barros, B.; Conde, B.; Cabaleiro, M.; Riveiro, B. Design and testing of a decision tree algorithm for early failure detection in steel truss bridges. *Eng. Struct.* **2023**, *289*, 116243. [CrossRef]
11. Katam, R.; Pasupuleti, V.D.K.; Kalapatapu, P. Machine learning-driven structural health monitoring: STFT-based feature extraction for damage detection. *Structures* **2025**, *78*, 109244. [CrossRef]
12. Cui, J.; Xie, P.; Wang, X.; Wang, J.; He, Q.; Jiang, G. M2FN: An end-to-end multi-task and multi-sensor fusion network for intelligent fault diagnosis. *Measurement* **2022**, *204*, 112085. [CrossRef]
13. Zhou, Y.; Zheng, Y.; Liu, Y.; Pan, T.; Zhou, Y. A hybrid methodology for structural damage detection uniting FEM and 1D-CNNs: Demonstration on typical high-pile wharf. *Mech. Syst. Signal Process.* **2022**, *168*, 108738. [CrossRef]
14. Das, T.; Guchhait, S. A 2D-CNN-based two-stage structural damage localization and quantification technique using time domain vibration data. *Int. J. Struct. Stab. Dyn.* **2024**, *24*, 2450232. [CrossRef]
15. Zhang, Z.K.; Meng, Q.M.; Cui, Z.K.; Yao, M.; Shao, Z.F.; Tao, B. Machine learning applications in parallel robots: A brief review. *Machines* **2025**, *13*, 565. [CrossRef]
16. Jia, Z.; Li, Z.F.; Wang, K.; Zhi, G.Z.; Liu, Z.B.; Vong, C.-M. Graph convolutional contrastive learning for few-shot open-set fault diagnosis in electro-hydrostatic actuators. *IEEE Trans. Aerosp. Electron. Syst.* **2026**, *62*, 3077–3090. [CrossRef]
17. Jia, Z.; Liu, Z.B.; Li, Z.F.; Wang, K.; Vong, C.-M. Lightweight fault diagnosis via siamese network for few-shot EHA circuit analysis. *IEEE Trans. Aerosp. Electron. Syst.* **2025**, *61*, 15585–15596. [CrossRef]
18. Hewawasam, H.; Kahandawa, G.; Ibrahim, Y. Machine learning-based agoraphilic navigation algorithm for use in dynamic environments with a moving goal. *Machines* **2023**, *11*, 513. [CrossRef]
19. Xu, Z.C.; Zhang, B.L.; Fan, L.L.; Yan, E.H.Z.; Li, D.F.; Zhao, Z.J.; Ye, W.S.; Xue, T. Deep-learning-driven intelligent tool wear identification of high-precision machining with multi-scale CNN-BiLSTM-GCN. *Adv. Eng. Inform.* **2025**, *65*, 103234. [CrossRef]

20. Liu, H.Y.; Sun, J.Z.; Pan, Y.C.; Hu, D.W.; Lei, S.; Xu, Z.S.; Yu, H.L.; Yang, L. Power supply risk identification method of active distribution network based on transfer learning and CBAM-CNN. *Energies* **2024**, *17*, 4438. [CrossRef]
21. Yan, Q.; Yang, Y.; Zhang, C.; Xiong, Z.; Zhong, H.; Xu, Y.; Yang, W. Intelligent monitoring of impact damage within concrete through deep learning-empowered electromechanical impedance technique. *Measurement* **2025**, *253*, 117642. [CrossRef]
22. Ma, Y.S.; Tian, Z.H.; Xu, X.B.; Liu, H.R.; Li, J.J.; Fan, H.Y. Research on response parameters and classification identification method of concrete vibration process. *Materials* **2023**, *16*, 2958. [CrossRef] [PubMed]
23. Liu, H.; Liu, C.Z.; Fu, J.K.; Ma, C.Z.; Zhang, Y.; Lei, Y.M. Intelligent analysis of hydraulic concrete vibration time based on convolutional neural network. *Adv. Civ. Eng.* **2023**, *2023*, 5530102. [CrossRef]
24. Tao, H.H.; Jia, P.; Wang, X.Y.; Wang, L.Q. Real-time fault diagnosis for hydraulic system based on multi-sensor convolutional neural network. *Sensors* **2024**, *24*, 353. [CrossRef] [PubMed]
25. Huang, K.K.; Wu, S.J.; Li, F.B.; Yang, C.H.; Gui, W.H. Fault diagnosis of hydraulic systems based on deep learning model with multirate data samples. *IEEE Trans. Neural Netw. Learn. Syst.* **2022**, *33*, 6789–6801. [CrossRef]
26. Wang, X.W.; Zhang, X.A.; Shahzad, M.M. A novel structural damage identification scheme based on deep learning framework. *Structures* **2021**, *29*, 1537–1549. [CrossRef]
27. Koopialipoor, M.; Asteris, P.G.; Mohammed, A.S.; Alexakis, D.E.; Mamou, A.; Armaghani, D.J. Introducing stacking machine learning approaches for the prediction of rock deformation. *Transp. Geotech.* **2022**, *34*, 100756. [CrossRef]
28. Senthil, G.A.; Prabha, R.; Arun, M.; Nisha, A.S.A.; Prabu, S. A novel predictive analysis and classification of land subsidence vulnerability mapping based on GIS using hybrid optimized machine learning techniques and computer vision. *Procedia Comput. Sci.* **2024**, *233*, 343–352. [CrossRef]
29. Liu, Z.Y.; Li, S.X.; Hao, J.L.; Hu, J.F.; Pan, M.Y. An efficient and fast model reduced kernel KNN for human activity recognition. *J. Adv. Transp.* **2021**, *2021*, 2026895. [CrossRef]
30. Moussa, H.; Elabeidy, A.B.; Akcaoglu, T. Predicting the compressive strength of rubberized concrete containing silica fume using stacking ensemble learning model. *Constr. Build. Mater.* **2024**, *449*, 138254. [CrossRef]
31. Wang, X.W.; Wang, Z.H.; Yang, S.X.; Wei, S.Q.; Wang, T.L.; Shahzad, M.M. An incremental broad ensemble learning framework for the identification of structural damage in conditions of data scarcity and non-stationarity. *Eng. Struct.* **2026**, *353*, 122261. [CrossRef]

Disclaimer/Publisher's Note: The statements, opinions and data contained in all publications are solely those of the individual author(s) and contributor(s) and not of MDPI and/or the editor(s). MDPI and/or the editor(s) disclaim responsibility for any injury to people or property resulting from any ideas, methods, instructions or products referred to in the content.